Journal of Biomedical Optics

BiomedicalOptics.SPIEDigitalLibrary.org

Dynamic *in vivo* imaging of small animal brain using pulsed laser diode-based photoacoustic tomography system

Paul Kumar Upputuri
Manojit Pramanik

SPIE.

Paul Kumar Upputuri, Manojit Pramanik, "Dynamic *in vivo* imaging of small animal brain using pulsed laser diode-based photoacoustic tomography system," *J. Biomed. Opt.* **22**(9), 090501 (2017), doi: 10.1117/1.JBO.22.9.090501.

Dynamic *in vivo* imaging of small animal brain using pulsed laser diode-based photoacoustic tomography system

Paul Kumar Upputuri and Manojit Pramanik*
Nanyang Technological University, School of Chemical and Biomedical Engineering, Singapore, Singapore

Abstract. We demonstrate dynamic *in vivo* imaging using a low-cost portable pulsed laser diode (PLD)-based photoacoustic tomography system. The system takes advantage of an 803-nm PLD having high-repetition rate ~7000 Hz combined with a fast-scanning single-element ultrasound transducer leading to a 5 s cross-sectional imaging. Cortical vasculature is imaged in scan time of 5 s with high signal-to-noise ratio ~48. To examine the ability for dynamic imaging, we monitored the fast uptake and clearance process of indocyanine green in the rat brain. The system will find applications to study neurofunctional activities, characterization of pharmacokinetic, and biodistribution profiles in the development process of drugs or imaging agents. [DOI: 10.1117/1.JBO.22.9.090501]

Keywords: photoacoustic tomography; *in vivo* imaging; brain imaging; contrast agent; high-speed imaging.

Paper 170391LR received Jun. 16, 2017; accepted for publication Sep. 5, 2017; published online Sep. 26, 2017.

1 Introduction

Small animals are important models for preclinical studies and play a key role in guiding the study of human diseases and in seeking effective treatment. The ideal small animal imaging technique should provide noninvasive, high spatiotemporal resolution, deep penetration, anatomical and functional contrasts.[1] The ability to directly visualize dynamics in small animal models at the full-body scale provides insights into biological processes at the whole-organism level. Optical imaging techniques suffer from either shallow penetration or a poor depth-to-resolution ratio; on the other hand, nonoptical imaging techniques for full-body imaging of small animals lack either spatiotemporal resolution or functional contrast.[2,3]

Photoacoustic tomography (PAT) is an emerging noninvasive, nonionizing, hybrid imaging modality that has found many demanding applications in both clinical and preclinical studies.[4,5] PAT combines the advantages of both optical and ultrasound imaging modalities: high optical contrast and scalable ultrasound resolution and imaging depth. In PAT, short laser pulses (nanosecond) are absorbed by tissue chromophores and produce an acoustic wave [also known as photoacoustic (PA) wave]. Images are formed by reconstructing the PA signals acquired at various positions around the tissue. Over the past couple of decades, PAT has been successfully used for animal and human imaging. PAT has shown its potential for imaging various organs (heart, lungs, liver, eyes, spleen, brain, skin, spinal cord, kidney, etc.)[6] in small animals. Multiple-wavelength PAT allows mapping of HbT—total hemoglobin concentration and SO_2—oxygen saturation. PAT can provide information at molecular and genetic levels for better understanding of brain health.[7] Photoacoustic microscopy (PAM) provides higher resolution imaging with sacrificed imaging depth and may also require scalp removal (minimally invasive).[8] Whereas, PAT can provide few cm imaging depth, and it is a complete noninvasive technique. Therefore, PAT systems were widely used for whole filed brain imaging.[9,10]

A Q-switched Nd:YAG-pumped optical parametric oscillator is the most commonly used excitation sources for PAT, as they provide sufficient pulse energies (tens-millijoules) with ~5 ns pulse widths at ~10 to 100 Hz repetition rate. If single ultrasound transducer (UST) scanning is used, the temporal resolution of a Nd:YAG-based PAT system is limited by the low repetition rate of the laser and scanning/rotation speed of the UST. Typically, few minutes or longer are normally required to acquire one cross-sectional *in vivo* PAT image.[11] A PAT system with such lengthy measurement time is not ideal for small animal imaging because it is difficult to control the physiological parameters for whole body imaging, time-resolved functional imaging, etc. Small animal neurofunctional imaging, oxygen saturation imaging, blood velocity imaging, etc. do require dynamic imaging capability. Monitoring the pharmacokinetic, circulation time of drugs/contrast agents is another important area where dynamic imaging is required.[12–14] If only one single-element UST is used to collect all the PA signals around the sample, it will limit the imaging speed of the system. Nd:YAG/PAT combined with multiple single-element USTs or array-bases USTs could achieve high-speed imaging. A multi-transducer PAT was demonstrated based on the electrical slip ring.[6] The lateral and axial resolution of the system was ~0.129 and ~1.49 mm, respectively. The scanning speed was 1.5 min/frame. In this system, electromagnetic shielding was a challenge for transmission of weak PA signals. A linear array-based PAT was demonstrated for full-view imaging.[15] The imaging resolution was ~60 μm, and the imaging speed was limited by the low repetition rate (20 Hz) of the laser and the slow manual rotation scan. A linear array-based PAT system was demonstrated for whole mouse brain imaging.[16] Imaging resolution of the system was ~70 μm and temporal resolution was 1 s. Several array-based USTs such as linear, semicircular, circular, and volumetric array are successfully used for real-time imaging.[4] These array-based USTs will increase the imaging speed, but they are expensive, require custom made electronics, and will reduce the measurement sensitivity. Moreover, the imaging speed of a PAT system that uses array-based USTs is still limited by the repetition rate of the excitation laser.

Recently, pulsed laser diodes (PLDs) and light emitting diodes[4,17,18] have been reported as compact and less expensive alternatives for Nd:YAG lasers. High-frame rate (7000 fps) B-scan PA imaging was shown with PLDs using clinical ultrasound platform.[19] PLD with high-repetition rate can improve

*Address all correspondence to: Manojit Pramanik, E-mail: manojit@ntu.edu.sg

1083-3668/2017/$25.00 © 2017 SPIE

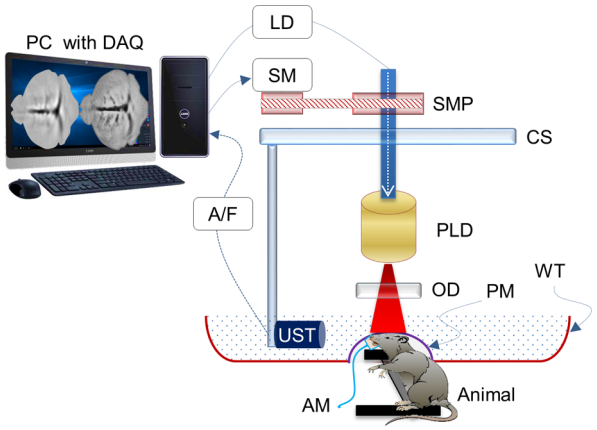

Fig. 1 Schematic of the PLD-PAT system for *in vivo* small animal brain imaging: PLD, pulsed laser diode; OD, optical diffuser; CS, circular scanning plate; SMP, stepper motor pulley unit; UST, ultrasound transducer; A/F, amplifier/filter unit; LD, laser driver unit; SM, stepper motor; PC, personal computer; WT, water tank; DAQ, data acquisition card; AM, anesthesia machine; PM, transparent polythene membrane.

the imaging speed of a PAT system even with single-element UST circular scanning (CS) geometry. Single-element USTs are less expensive and highly sensitive unlike array-based USTs. Few research works were reported on using high-repetition rate PLDs as an excitation source for PA imaging. A fiber-based near infrared PLD was demonstrated for PA imaging on phantoms.[20] *In vivo* imaging of blood vessels at ~1-mm-depth below the human skin was demonstrated using low-energy PLDs.[21] A PLD-based optical resolution photoacoustic microscopy (ORPAM) was reported. Using PLDs, ~1.5-cm-deep imaging at a frame rate of 0.43 Hz was demonstrated.[22] A low-cost photoacoustic computer tomography (LC-PACT) system was demonstrated for *ex vivo* imaging. The system uses 6 W 905-nm PLD, emitting 55 ns pulses at 20 kHz with 0.3 mJ pulse energy. The image of black tape acquired using LC-PACT in 30 s showed 5.4 dB signal-to-noise ratio (SNR).[23] We reported a low-cost portable photoacoustic tomography (PLD-PAT) system for high-speed imaging.[11,24] The system could provide hair phantom images in 3 s (with SNR 29 dB) and 30 s (with SNR 38 dB). The imaging speed and SNR of a PLD-PAT system in Ref. 11 are much higher than that presented in Ref. 23. In these letters, we report our studies of high-speed *in vivo* imaging on a small animal brain using a PLD-PAT system. We compare the *in vivo* brain images acquired at different scan speeds. To examine the high-speed, we monitored the fast uptake and clearance process of indocyanine green (ICG) in the cortical region of rat brain.

The schematic of the *in vivo* PLD-PAT imaging system is shown in Fig. 1. The PLD (Quantel, France) provides ~136 ns pulses at ~803 nm wavelength, and ~1.4 mJ pulse energy (@ 7 kHz repetition rate). An optical diffuser (OD) was used to make the PLD beam more homogenous. The PLD was controlled by the laser driver (LD). The LD included a temperature controller (LaridTech, MTTC1410), a 12 V power supply (Voltcraft, PPS-11810), a variable power supply (BASETech, BT-153), and a function generator (FG250D, Funktionsgenerator). The function generator synchronizes data acquisition (DAQ) with the laser excitation. The animal brain and the UST were mounted as shown in Fig. 1. A cylindrically focused UST (V306-SU-NK-CF1.9IN Olympus NDT) of 2.25 MHz central frequency (70% fractional bandwidth), 13 mm active area, and focal length of 1.9 in. was used. The UST was driven by a step motor (SM) (Lin Engineering, Silverpak 23C) to circularly scan around the brain. The UST holder was mounted on a CS plate. The motion of the circular plate or UST was controlled by the computer-controlled SM. The UST detected signals were amplified, bandpass filtered by ultrasound signal receiver (A/F) unit (Olympus-NDT, 5072PR), and then digitized and recorded by the PC with DAQ card (25 Ms/s, GaGe, compuscope 4227).

The maximum permissible exposure (MPE) limit for *in vivo* imaging is governed by the American National Standards Institute (ANSI). In the 700- to 1050-nm wavelength range, the energy density on the skin by single pulse should be $<20 \times 10^{2(\lambda-700)/1000}$ mJ/cm^2 [λ(nm)].[25] For 803-nm wavelength, the limit is ~31 mJ/cm^2. If laser is exposed continuously over a period of $t = 5$ s, then the MPE becomes $1.1 \times 10^{2(\lambda-700)/1000} \times t^{0.25}$ J/cm^2 (=2.6 J/cm^2). For *in vivo* imaging, the PLD was operated at 7000 Hz. In 5-s scan time, total 35000 (i.e., 5×7000) pulses were delivered to the sample, so per pulse the MPE is 0.074 mJ/cm^2. The pulse energy was ~1.4 mJ at laser window when the laser was operated at maximum power 10 W and repetition rate 7000 Hz. For *in vivo* imaging, pulse energy achieved on the tissue surface was ~0.86 mJ distributed over 12-cm^2 area. So, the energy density is ~0.071 mJ/cm^2 (0.86 mJ/12 cm^2), which was within the ANSI limit 0.074 mJ/cm^2 for 5 s scan time.

For *in vivo* animal experiments, NTac:Sprague Dawley®SD® female healthy rats of body weight ~95 ± 3 gm, procured from InVivos Pte. Ltd., Singapore, were used. Experiments were performed in accordance with the guidelines and regulations approved by the Institutional Animal Care and Use Committee of Nanyang Technological University, Singapore (ARF-SBS/NIE-A0263). The rat was anesthetized with a mixture of 2 ml of Ketamine (100 mg/ml), 2 ml of xylazine (20 mg/ml), and 1 ml of saline. Before going for imaging, the hair on the scalp was depilated. The animal was mounted in the system as shown in Fig. 1. A custom-designed animal holder was used to mount the animal. The animal was placed in sitting position, on its abdomen, and the body of the animal was secured to the mount with surgical tapes to provide grip for the animal. The mouth and nose of the animal were covered with a breathing mask to deliver anesthesia mixture during the experiment. The anesthesia was achieved by the continuous inhalation of a mixture of 1.0 L/ min oxygen and 0.75% isoflurane. The animal brain was aligned to the center of the CS geometry. After completing the DAQ for imaging, the animal was euthanized by an intraperitoneal injection of pentobarbital of concentration 300 mg/ml.

We noninvasively imaged the brains of healthy rats using the high-speed *in vivo* PLD-PAT system. The rat was placed at the center of the laser illumination area and CS area. The A-lines signals from the rat brain area were acquired by continuously scanning the UST at predefined speed. Multiple PA signals were collected by the UST, the collected signals were preamplified with gain of 50 dB, and finally the amplified A-lines were saved once the rotation is complete. PA signals can be averaged later if needed. We acquired the PA signals from brain area in different scan times. The photograph of the brain taken before and after opening the scalp is shown in Figs. 2(a) and 2(b), respectively. An open scalp anatomical photograph of the cortex vasculature was taken after removing the scalp for comparison. PAT imaging was done noninvasively, i.e., with skin and skull intact. The reconstructed PAT cross-sectional images of the rat

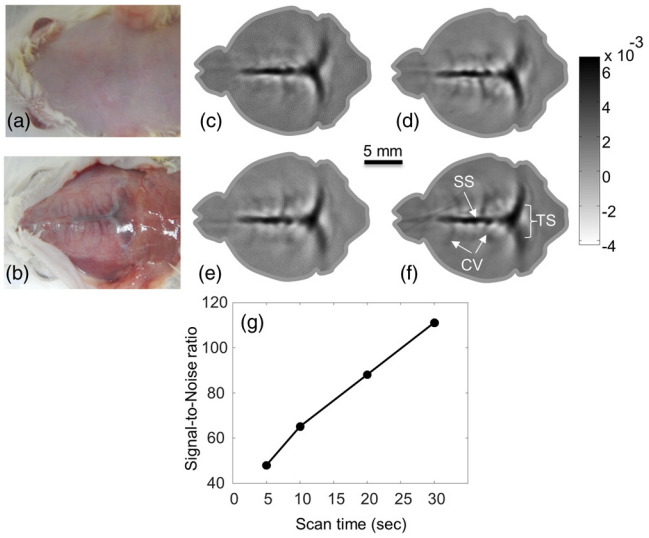

Fig. 2 Noninvasive images of brain vasculature in 95 gm female rat at different scan times: photograph of rat brain before (a) and after (b) removing the scalp. *In vivo* brain images at (c) 5-s, (d) 10-s, (e) 20-s, and (f) 30-s scan time. (g) SNR of *in vivo* images as a function of scan time. Here, SS, sagittal sinus; TS, transverse sinus; and CV, cerebral veins.

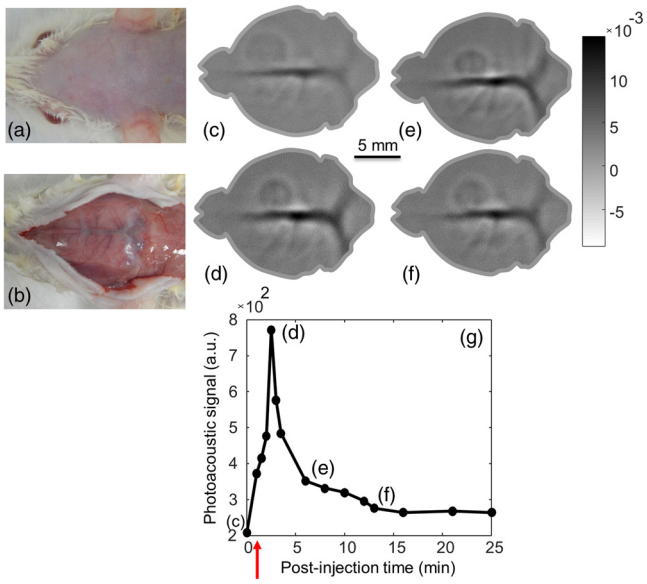

Fig. 3 *In vivo* PLD-PAT brain imaging and pharmacokinetics of ICG intravenously injected in to rat brain: photograph of rat brain before (a) and after (b) removing the scalp. *In vivo* brain images at different scan times (c) 0 s, (d) 2 min, (e) 6 min, and (f) 13 min. (g) Graph shows the quantification of ICG signal in the superior SS during 25 min following injection. The red arrow indicates ICG injection point.

brain obtained by collecting PA signals in 30-, 20-, 10-, and 5-s scan time are shown in Figs. 2(c)–2(f). Reconstruction was done using a simple delay-and-sum algorithm.[26,27] In all the PAT cross-sectional images, the superior sagittal sinus (SS), transverse sinuses (TS), and cerebral veins (CV) of the rat brain are clearly visible. To study the effect of scan speed on the quality of the *in vivo* images, we calculated the SNR of images acquired at different scan speeds. The SNR was defined as the peak-to-peak amplitude of the PA signal divided by the standard deviation of the noise, $\mathrm{SNR} = V/n$, where V is the peak-to-peak PA signal amplitude, and n is the standard deviation of the background noise. The SNR as a function of scan time is shown in Fig. 2(g). This experiment was done to compare the *in vivo* images at different scan speeds and to prove that even 5-s scanning time was enough to get high-quality brain images.

To examine the ability for high-speed brain imaging, ICG (12633-25mg, SigmaAldrich) was injected into the tail vein and the uptake and clearance of ICG were monitored by a PLD-PAT system in the vasculature of the brain dynamically. The photograph of the rat brain before and after opening the scalp is shown in Figs. 3(a) and 3(b), respectively. Before the administration of ICG, the cortical vascular structure was imaged noninvasively at 5-s scan time as shown in Fig. 3(c). To monitor the wash-in process of the dye, about 0.3 ml of ICG at 323 μM concentration was administered through tail vein injection.[11] The entire cortical region was imaged at 5-s scan time. As shown in Fig. 3(c), the control image obtained before the injection has low contract. With the increase in the optical absorption by ICG at 803-nm wavelength, the vascular contrast started increasing, as shown in Figs. 3(d)–3(f). The ICG dye in the blood vessels helped to recover fine vascular structures in the PA image at 803-nm wavelength. Figure 3(g) shows the measured increase and subsequent decrease in ICG signal in the superior SS over time. We observed same trend on multiple rats. This trend is similar to the one reported in Ref. 28. The uptake of ICG was maximum at ~2- min postinjection and the clearance process of the dye was monitored for 25 min after injection. The increase in the PA values indicates the increase in the dye concentration within the cortex vessels. To generate the plot in Fig. 3(g), images were not acquired continuously. One PAT image in every ~30 s or so was acquired, that means the laser was ON for 5 s and OFF for the rest 25 s.

In this letter, we demonstrated an affordable and portable PLD-PAT system for high-speed and high-quality *in vivo* imaging on small animals. The potentiality of the system for dynamic *in vivo* imaging was demonstrated by monitoring a fast uptake and clearance process of ICG in the cortex vasculature. The *in vivo* brain images were acquired in scan time as short as 5 s with high SNR ~48 using a single-element UST scanner. The temporal resolution can be improved using multiple UST and instead of rotating a full circle of 360 deg, one can rotate only 360/N deg (where, N is the number of USTs used). For example, if eight USTs are used, then imaging can be done at one frame per ~0.5 s. The spatial resolution of the current PLD-PAT system is ~384 μm (for 2.25 MHz transducer) and ~185 μm (for 5 MHz transducers).[11] The spatial resolution can be further improved using UST with higher central frequency and bandwidth. Although ring PA systems[29] can provide real-time PA imaging, they are custom made and very expensive. The portability, low-cost, image quality promises that the proposed system will find applications in neurofunctional activities (such as epilepsy), characterization of pharmacokinetic, biodistribution profiles in the development process of drugs or imaging agents in small animal study.

Disclosures

Authors have no relevant financial interests in this work and no other potential conflicts of interest to disclose.

Acknowledgments

The authors would like to acknowledge the financial support from the Singapore Ministry of Health's National Medical

Research Council (NMRC/OFIRG/0005/2016: M4062012) and Ms. Vijitha Periyasamy for assisting in the animal experiments.

References

1. L. Li et al., "Single-impulse panoramic photoacoustic computed tomography of small-animal whole-body dynamics at high spatiotemporal resolution," *Nat. Biomed. Eng.* **1**, 0071 (2017).
2. P. K. Upputuri et al., "Recent developments in vascular imaging techniques in tissue engineering and regenerative medicine," *BioMed Res. Int.* **2015**, 1–9 (2015).
3. J. Xia and L. V. Wang, "Small-animal whole-body photoacoustic tomography: a review," *IEEE Trans. Biomed. Eng.* **61**(5), 1380–1389 (2014).
4. P. K. Upputuri and M. Pramanik, "Recent advances toward preclinical and clinical translation of photoacoustic tomography: a review," *J. Biomed. Opt.* **22**(4), 041006 (2017).
5. L. V. Wang and S. Hu, "Photoacoustic tomography: in vivo imaging from organelles to organs," *Science* **335**(6075), 1458–1462 (2012).
6. Z. Deng, W. Li, and C. Li, "Slip-ring-based multi-transducer photoacoustic tomography system," *Opt. Lett.* **41**(12), 2859–2862 (2016).
7. J. J. Yao et al., "Noninvasive photoacoustic computed tomography of mouse brain metabolism in vivo," *NeuroImage* **64**(1), 257–266 (2013).
8. J. Yao et al., "High-speed label-free functional photoacoustic microscopy of mouse brain in action," *Nat. Methods* **12**(5), 407–410 (2015).
9. J. Yao, J. Xia, and L. V. Wang, "Multiscale functional and molecular photoacoustic tomography," *Ultrason. Imaging* **38**(1), 44–62 (2016).
10. I. Olefir et al., "Hybrid multispectral optoacoustic and ultrasound tomography for morphological and physiological brain imaging," *J. Biomed. Opt.* **21**(8), 086005 (2016).
11. P. K. Upputuri and M. Pramanik, "Performance characterization of low-cost, high-speed, portable pulsed laser diode photoacoustic tomography (PLD-PAT) system," *Biomed. Opt. Express* **6**(10), 4118–4129 (2015).
12. C. Xie et al., "Self-quenched semiconducting polymer nanoparticles for amplified in vivo photoacoustic imaging," *Biomaterials* **119**, 1–8 (2017).
13. Y. Jiang et al., "Broadband absorbing semiconducting polymer nanoparticles for photoacoustic imaging in second near-infrared window," *Nano Lett.* **17**(8), 4964–4969 (2017).
14. A. Taruttis et al., "Fast multispectral optoacoustic tomography (MSOT) for dynamic imaging of pharmacokinetics and biodistribution in multiple organs," *PLoS One* **7**(1), e30491 (2012).
15. G. Li et al., "Multiview Hilbert transformation for full-view photoacoustic computed tomography using a linear array," *J. Biomed. Opt.* **20**(6), 066010 (2015).
16. P. Zhang et al., "High-resolution deep functional imaging of the whole mouse brain by photoacoustic computed tomography *in vivo*," *J. Biophotonics*, 1–6 (2017).
17. X. Dai, H. Yang, and H. Jiang, "*In vivo* photoacoustic imaging of vasculature with a low-cost miniature light emitting diode excitation," *Opt. Lett.* **42**(7), 1456–1459 (2017).
18. J. T. Allen and C. P. Beard, "High power visible light emitting diodes as pulsed excitation sources for biomedical photoacoustics," *Biomed. Opt. Express* **7**(3), 1260–1270 (2016).
19. K. Sivasubramanian and M. Pramanik, "High frame rate photoacoustic imaging at 7000 frames per second using clinical ultrasound system," *Biomed. Opt. Express* **7**(2), 312–323 (2016).
20. J. S. Allen and P. Beard, "Pulsed near-infrared laser diode excitation system for biomedical photoacoustic imaging," *Opt. Lett.* **31**(23), 3462–3464 (2006).
21. R. G. M. Kolkman, W. Steenbergen, and T. G. van Leeuwen, "*In vivo* photoacoustic imaging of blood vessels with a pulsed laser diode," *Lasers Med. Sci.* **21**(3), 134–139 (2006).
22. K. Daoudi et al., "Handheld probe integrating laser diode and ultrasound transducer array for ultrasound/photoacoustic dual modality imaging," *Opt. Express* **22**(21), 26365–26374 (2014).
23. A. Hariri et al., "Development of low-cost photoacoustic imaging systems using very low-energy pulsed laser diodes," *J. Biomed. Opt.* **22**(7), 075001 (2017).
24. P. K. Upputuri and M. Pramanik, "Pulsed laser diode based optoacoustic imaging of biological tissues," *Biomed. Phys. Eng. Express* **1**(4), 045010 (2015).
25. American National Standard for Safe Use of Lasers, ANSI Standard Z136.1-2000, Laser Institute of America, New York (2000).
26. S. K. Kalva and M. Pramanik, "Experimental validation of tangential resolution improvement in photoacoustic tomography using a modified delay-and-sum reconstruction algorithm," *J. Biomed. Opt.* **21**(8), 086011 (2016).
27. M. Pramanik, "Improving tangential resolution with a modified delay-and-sum reconstruction algorithm in photoacoustic and thermoacoustic tomography," *J. Opt. Soc. Am. A* **31**(3), 621–627 (2014).
28. N. C. Burton et al., "Multispectral opto-acoustic tomography (MSOT) of the brain and glioblastoma characterization," *NeuroImage* **65**(2), 522–528 (2013).
29. C. Li et al., "Real-time photoacoustic tomography of cortical hemodynamics in small animals," *J. Biomed. Opt.* **15**(1), 010509 (2010).